Asian Journal of Chemistry; Vol. 37, No. 4 (2025), 918-924

ASIAN JOURNAL OF CHEMISTRY

https://doi.org/10.14233/ajchem.2025.33505

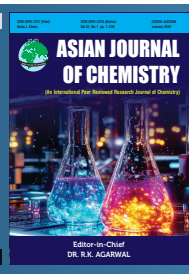

Facile Synthesis of Single Phase Pr-Doped $BiFeO_3$ Nanoparticles *via* a Sol-Gel Auto Combustion Technique

SWETANGI SUMAN[1], DILIP KUMAR CHOUDHARY[1] and SIMANT KUMAR SRIVASTAV[2,*]

[1]University Department of Chemistry, Lalit Narayan Mithila University, Darbhanga-846004, India
[2]Department of Chemistry, University of Allahabad, Prayagraj-211002, India

*Corresponding author: E-mail: simant.iitk@gmail.com

Received: 13 February 2025; *Accepted*: 19 March 2025; *Published online*: 29 March 2025; AJC-21953

In this study, the synthesis of single-phase Pr-doped bismuth ferrite, $Bi_{1-x}Pr_xFeO_3$ (x = 0, 0.05, 0.07 and 0.10) nanoparticles by the sol-gel auto-combustion method, followed by calcination at 400 ºC, is reported. Thermogravimetric analysis (TGA), Fourier transform infrared spectroscopy (FT-IR), transmission electron microscopy (TEM) and X-ray diffraction (XRD) techniques were used to characterize the samples. TEM images illustrate the formation nearly spherical nanoparticles in the size range of 30-80 nm. XRD confirmed the formation of single phase and well-crystallized $Bi_{1-x}Pr_xFeO_3$ nanoparticles at 400 ºC. XRD results show a gradual shift and merge of diffraction peaks on increasing doping concentration of Pr^{3+} in the $BiFeO_3$ matrix, which suggested a structural phase transition.

Keywords: Bismuth ferrite, Sol-gel, Autocumbustion, Nanoparticles.

INTRODUCTION

The interest in perovskite bismuth ferrite ($BiFeO_3$) has increased in recent years due to its exceptional physical properties, including a notably high Curie temperature ($T_C \approx 1100$ K) as well as Néel temperature $T_N \approx 643$ K) [1]. These characteristics make $BiFeO_3$ an excellent candidate for room temperature multiferroic materials, which have promising applications in fields of spintronic devices [2,3]. Beyond its multiferroic properties, $BiFeO_3$ has also emerged as a potential visible-light-driven photocatalyst for the degradation of organic dye due to its small band gap (~2.0-2.5 eV) [4]. The small band gap, chemical stability and intrinsic electric polarization field of $BiFeO_3$ provide a foundation for photocatalytic activity under visible light [4-6]. Despite these advantages, the practical application of $BiFeO_3$ in photocatalysis remains limited due to the rapid recombination of photogenerated electron-hole pairs, which significantly reduces its photocatalytic efficiency [7]. Therefore, it is an interesting task to improves the photocatalytic activity of $BiFeO_3$ for practical use.

To achieve this purpose there are many innovative strategies that are used to overcome the limitations of rapid electron-hole recombination in $BiFeO_3$ and enhance its photocatalytic performance. Some of these approaches are as follows: creating nanoscale morphologies of $BiFeO_3$ to increase its surface area and provide more active sites for photocatalytic reactions. Introducing suitable dopants into the $BiFeO_3$ lattice to reform its electronic structure, enhance light absorption and suppress electron-hole recombination, forming heterojunctions with complementary semiconductors to facilitate efficient charge transfer and separation and modifying the surface properties to improve adsorption of reactants and stabilize charge carriers [8-11]. Recently, it has been investigated that among the above approaches, the doping at either the Bi or Fe site of the $BiFeO_3$ lattice plays a crucial role in altering its properties. In this regard, rare earth element doping has gained significant attention in modifying the properties of $BiFeO_3$. Rare earth dopants can act as trapping sites for electrons or holes, promoting the separation and efficient production of photogenerated charge carriers during photocatalytic reactions and increasing photocatalytic properties [12,13].

Doping with foreign atoms, such as dysprosium, gadolinium or manganese, at the Bi or Fe sites of the $BiFeO_3$ lattice has demonstrated notable improvements in photocatalytic activity [14-16]. For instance, Sakar *et al.* [14] reported that substituting Bi^{3+} with Dy^{3+} in $BiFeO_3$ resulted in a significant

enhancement in photocatalytic performance under visible light irradiation. Zhang *et al.* [16] reported that the photocatalytic activity of $BiFeO_3$ was enhanced by the doping of Gd. Despite these advancements, research on rare earth doping in $BiFeO_3$ for photocatalytic applications is still in its infancy, with numerous challenges remaining.

In many challenges, one big challenge is the preparation of phase pure and doped bismuth ferrite nanoparticles. $BiFeO_3$ is stable at a very narrow temperature range, hence, it is challenging to synthesize it with controlled structural features and high surface area [5,17]. To date, a number of techniques have been tried to synthesize nanosized $BiFeO_3$ such as solid-state reaction, co-precipitation, sonochemical, solution combustion and sol-gel process [18,19]. However, there are some drawbacks to these methods as they are either complex or require high calcination temperatures. Due to high calcination temperature, bismuth is lost due to volatilization, which results in the formation of impurity phases like $Bi_2Fe_4O_9$, $Bi_{36}Fe_{24}O_{57}$, Bi_2O_3, *etc*. along with the formation of $BiFeO_3$ phase [20]. Among these, the sol-gel approach has an advantage over other methods because the material synthesized by this method has a good surface area, good homogeneity and precise control over stoichiometry.

In this method, different types of complexing agents have been used to synthesize $BiFeO_3$ nanoparticles. For example, Park *et al.* [21] synthesized $BiFeO_3$ nanopowder of different particle sizes using ethylene glycol as a complexing agent. Liu *et al.* [22,23] used polyvinyl alcohol and glycerol as complexing agents to synthesize pure $BiFeO_3$ phase at 400 ºC. Similarly, Ghosh *et al.* [24] synthesized phase pure $BiFeO_3$ powder using tartaric acid as a complexing agent. Further, it is observed that when a weaker complexing agent is replaced by a stronger complexing agent (EDTA, succinic acid) phase pure $BiFeO_3$ is not formed [20]. Therefore, it is reasonable to speculate that a weaker complexing agent may be utilized for the synthesis of phase pure $BiFeO_3$.

Future studies are needed to optimize doping strategies and investigate the relation between the dopant concentration, structural changes and property alteration in order to fully utilize the potential of doped $BiFeO_3$. Keeping all the above perspectives in mind, in this work, we synthesized phase pure $BiFeO_3$ and 5%, 7% and 10% Pr-doped $BiFeO_3$ nanoparticles using a facile sol-gel autocombustion method using propylene glycol as a complexing agent, followed by calcination at 400 ºC. The crystal structure and morphologies were also investigated.

EXPERIMENTAL

Analytical grade bismuth nitrate pentahydrate ($Bi(NO_3)_3 \cdot 5H_2O$, 99.99%), ferric nitrate nonahydrate ($Fe(NO_3)_3 \cdot 9H_2O$, 99.95%) and praseodymium nitrate hexahydrate ($Pr(NO_3)_3 \cdot 6H_2O$, 99.9%) were procured from Sigma-Aldrich, USA. Nitric acid (69%) was procured from Merck and propylene glycol ($C_3H_8O_2$) was supplied from Thermofisher. For the preparation of bismuth ferrite nanoparticles, 3 mmol of bismuth nitrate pentahydrate was dissolved in 50 mL of dilute nitric acid. Similarly, 3 mmol of ferric nitrate nonahydrate was dissolved in 50 mL of distilled water in a separate beaker. Both solutions were then mixed to form 100 mL precursor solution, which was kept on a magnetic stirrer for heating and stirring. During continuous heating, 1 mL of propylene glycol was added as a complexing agent. The mixture was then heated between 100-120 ºC while being continuously stirred to remove any excess water. As water evaporates and the viscosity of the solution increases, gel formation occurs. Subsequently, after auto combustion a brown powder was obtained. The brown powder was then scratched out from the beaker and ground into a fine powder to obtain the $BiFeO_3$ precursor powder. Finally, this precursor powder was calcined at 400 ºC for 2 h in a muffle furnace to obtain well-crystallized $BiFeO_3$ nanoparticles.

Further, for the synthesis of 5%, 7% and 10% Pr-doped bismuth ferrite nanoparticles $Bi_{1-x}Pr_xFeO_3$ (x = 0.05, 0.07 and 0.10), bismuth nitrate pentahydrate, ferric nitrate nonahydrate and praseodymium nitrate are used in stoichiometric proportions. For example, to synthesize 3 mmol of $Bi_{0.95}Pr_{0.05}FeO_3$, 1.382 g of bismuth nitrate was dissolved into dil. nitric acid solution, 1.212 g of ferric nitrate and 0.065 g of praseodymium nitrate were dissolved in distilled water. Once all metal nitrate solutions were prepared and then combined to form a precursor solution followed by the addition of 1 mL of propylene glycol. This mixture was stirred continuously at 100-120 ºC until all the liquid evaporates, forming a gel-like fluid. As the process continues, the gel transforms into a fluffy precursor powder. Finally, this precursor powder undergoes calcination in a muffle furnace at 400 ºC for 2 h. This step ensures the formation of well-crystallized $Bi_{0.95}Pr_{0.05}FeO_3$ nanoparticles, which can then be characterized and used for further applications. Similarly, we synthesized $Bi_{0.93}Pr_{0.07}FeO_3$ and $Bi_{0.90}Pr_{0.10}FeO_3$.

Characterization: The precursors were subjected to thermogravimetric analysis (TGA) using a Mettler Toledo Star System TGA apparatus up to 850 ºC under ambient atmospheric conditions. Fourier transform infrared (FT-IR) spectra were recorded in the range of 400-4000 cm^{-1} using Bruker Vertex 70. X-ray diffraction (XRD) studies were carried out using X'Pert Pro, PANalytical over a 2θ range of 20º to 60º. Transmission electron microscopy (TEM) studies were carried out using FEI Technai G^2 U-Twin.

RESULTS AND DISCUSSION

TGA analysis: Fig. 1 shows the thermal decomposition of the $BiFeO_3$ and $Bi_{0.90}Pr_{0.10}FeO_3$ precursor powder. The TGA curve displays several stages of decomposition of the complex which is most likely formed during the reaction, such as the loss of carbonized, non-carbonized and water molecules and it shows an overall weight loss of 41% and 43% for $BiFeO_3$ and $Bi_{0.90}Pr_{0.10}FeO_3$ precursor, respectively. There is no noticeable weight loss beyond 400 ºC which suggests the phase formation temperature of pure and Pr-doped $BiFeO_3$ is 400 ºC.

FT-IR analysis: Fig. 2 shows the FT-IR spectra of pure and Pr-doped $BiFeO_3$ nanoparticles calcined at 400 ºC for 2 h. The band near 3400 cm^{-1} in all samples is assigned to anti-symmetric stretching in O-H from adsorbed water due to the contact of the samples with the environment. The bands at about 548 cm^{-1} and 445 cm^{-1} in $BiFeO_3$ can be assigned, respectively, to the mode ν of stretching vibrations along the Fe-O axis, to

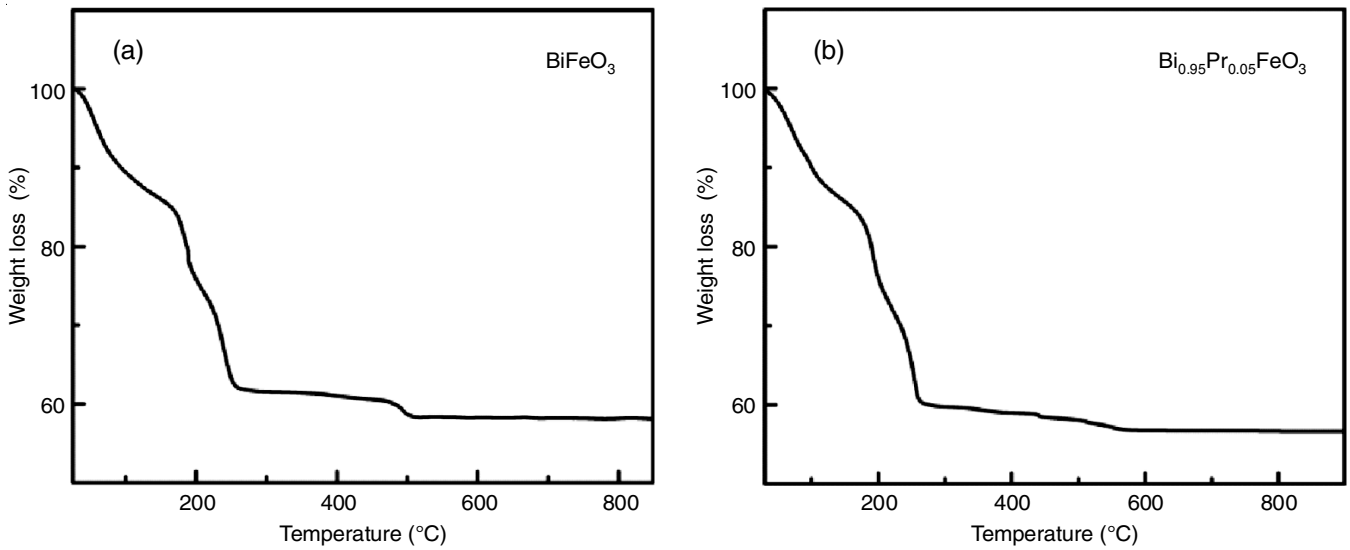

Fig. 1. (a) Thermograms of $BiFeO_3$ precursor powder (a) and $Bi_{0.90}Pr_{0.10}FeO_3$ precursor powder (b)

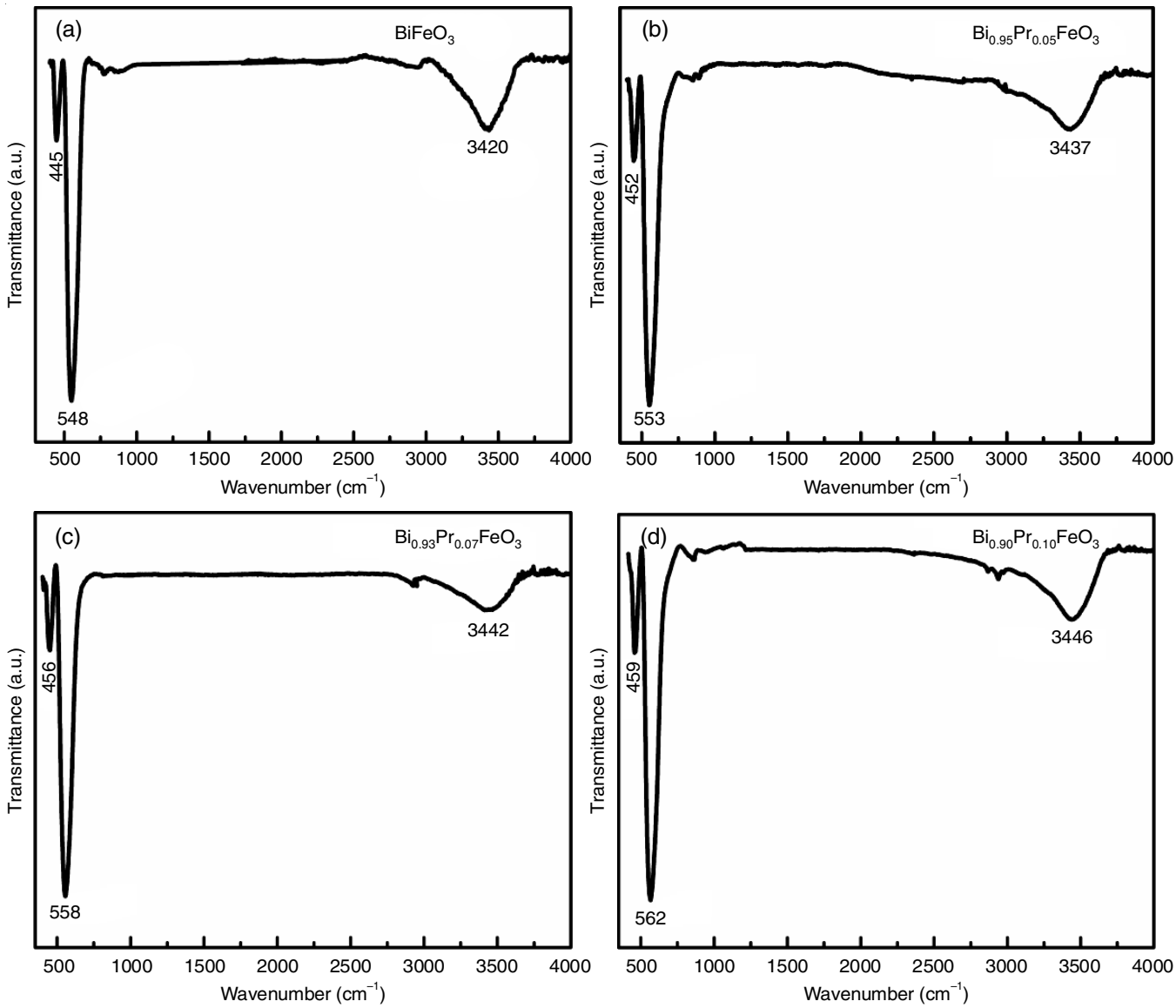

Fig. 2. FTIR spectra for (a) $BiFeO_3$, (b) $Bi_{0.95}Pr_{0.05}FeO_3$, (c) $Bi_{0.93}Pr_{0.07}FeO_3$ and (d) $Bi_{0.90}Pr_{0.10}FeO_3$ nanoparticles calcined at 400 ºC

δ distortional vibrations of O-Fe-O angles of the octahedral FeO_6 group in the perovskite compounds [25,26]. The IR frequencies of the bands 548 cm^{-1} and 445 cm^{-1} in $BiFeO_3$ shift to higher frequencies on increasing the Pr concentration (Fig. 2). The IR bands at 548 cm^{-1} and 445 cm^{-1} in $BiFeO_3$ shifts to 553 cm^{-1} and 452 cm^{-1} in $Bi_{0.95}Pr_{0.05}FeO_3$, 558 cm^{-1} and 456 cm^{-1} in $Bi_{0.93}Pr_{0.07}FeO_3$ and 562 cm^{-1} and 459 cm^{-1} in $Bi_{0.90}Pr_{0.10}FeO_3$, respectively. This behaviour is attributed to the change in the reduced mass of the Fe-O oscillator with increasing Pr-content.

TEM analysis: Fig. 3 shows a typical TEM image of pure and Pr-doped $BiFeO_3$ nanoparticles synthesized at 400 ºC. It is evident that the size of synthesized pure and Pr-doped $BiFeO_3$ particles are in the range of 30 to 80 nm and roughly spherical in shape. This clearly confirms the nanocrystalline nature of all the synthesized samples and samples are polycrystalline in nature.

XRD analysis: Powdered X-ray diffraction (XRD) was employed to analyze the phase and the crystal structure of the synthesized $Bi_{1-x}Pr_xFeO_3$ nanoparticles (where x = 0.0, 0.05, 0.07, 0.10). Fig. 4 shows the XRD patterns of pure and Pr-doped $BiFeO_3$ nanoparticles in the 2θ range between 20º to 60º at room temperature. The XRD pattern of the synthesized $BiFeO_3$ nanoparticles closely matches the standard JCPDS card no. 86-1518, which corresponds to the rhombohedral crystal structure with *R*3*c* space group of the $BiFeO_3$ phase. The characteristic peaks in the XRD pattern of $BiFeO_3$ appear at specific 2θ values of 22.43º, 31.77º, 32.09º, 37.67º, 38.97º, 39.50º, 45.77º, 51.34º, 51.77º, 56.38º and 57.03º, corresponding to the (012), (104), (110), (113), (006), (202), (024), (116), (112), (018) and (214) planes, respectively. From Fig. 4b-d, it is clear that the XRD pattern of the 5%, 7% and 10% of Pr-substituted $BiFeO_3$ nanoparticles closely resemble with the XRD pattern of the pure phase of $BiFeO_3$ nanoparticles. There is no additional diffraction peak appeared in the Pr-doped samples, which indicates the absence of secondary impurities or other phases in the synthesized samples. This confirms the effective dispersion

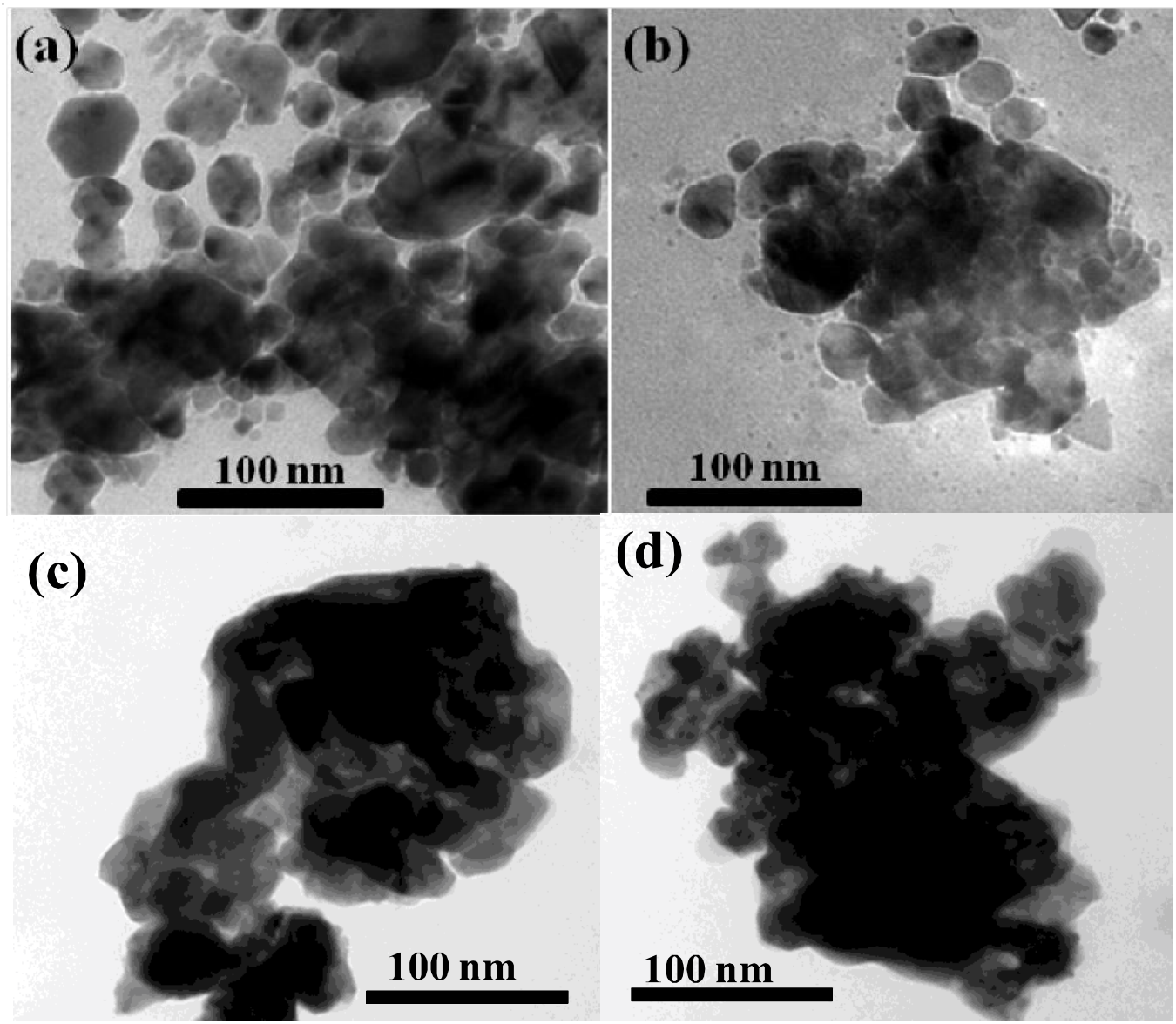

Fig. 3. TEM images of (a) $BiFeO_3$, (b) $Bi_{0.95}Pr_{0.05}FeO_3$, (c) $Bi_{0.93}Pr_{0.07}FeO_3$ and (d) $Bi_{0.90}Pr_{0.10}FeO_3$ nanoparticles calcined at 400 ºC

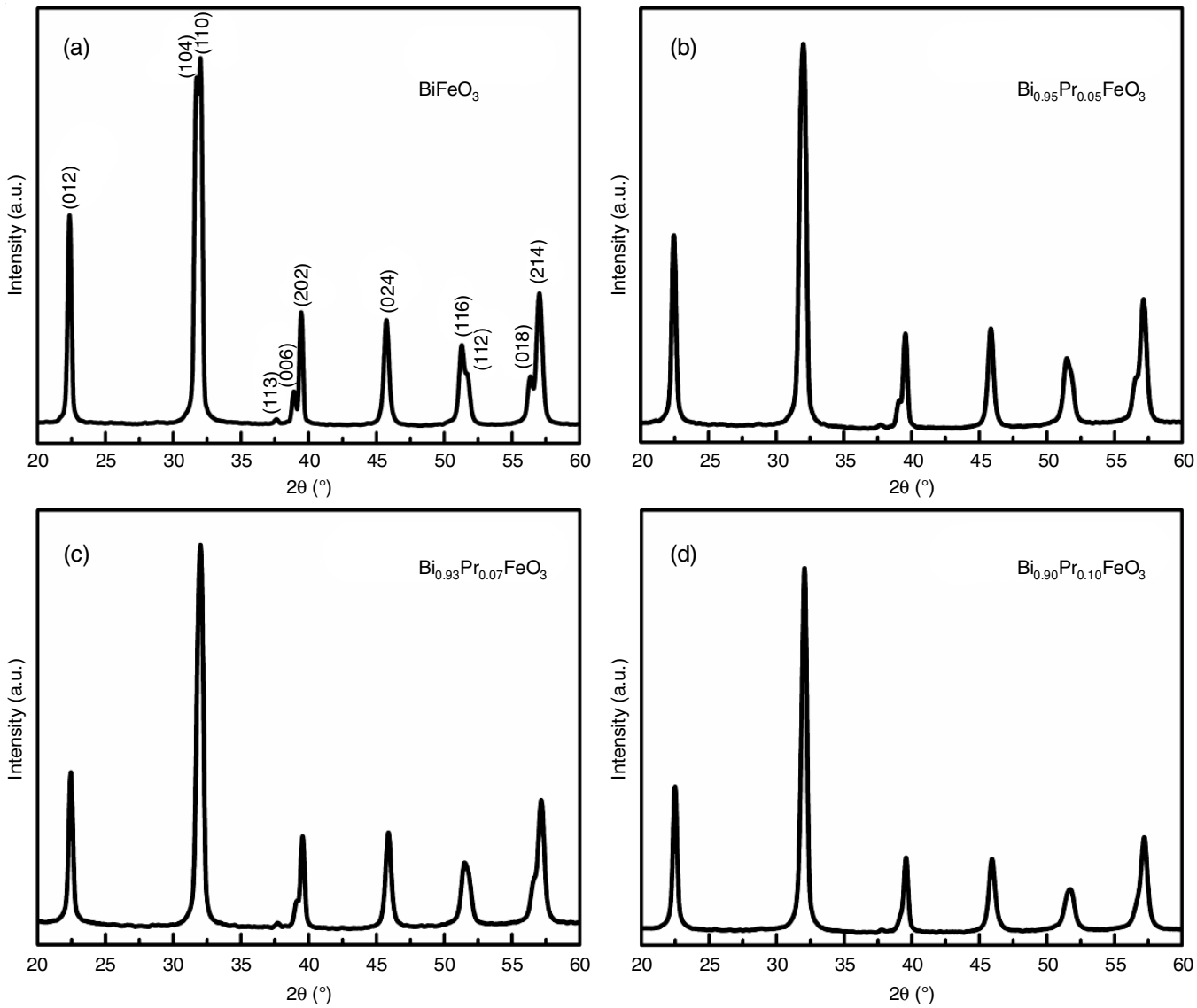

Fig. 4. XRD pattern of (a) $BiFeO_3$, (b) $Bi_{0.95}Pr_{0.05}FeO_3$, (c) $Bi_{0.93}Pr_{0.07}FeO_3$ and (d) $Bi_{0.90}Pr_{0.10}FeO_3$ nanoparticles calcined at 400 ºC

of the Pr dopant within the $BiFeO_3$ host matrix and the successful formation of pure Pr-doped $BiFeO_3$ nanoparticles.

Further, there are two important effects of the Pr-doping in the $BiFeO_3$ matrix as observed in Fig. 4i. The diffraction peaks gradually shifted towards the higher 2θ and (ii) the splitted diffraction peaks in pure $BiFeO_3$ continuously merged in single peak on increasing Pr-concentration in $BiFeO_3$ matrix. To make these observations clearer, magnified XRD patterns in the vicinity of 2θ around 32º, 39º, 51º and 57º are shown in Fig. 5. It is confirmed that diffraction peaks corresponding to the *hkl* planes [(110) and (104)], [(006) and (202)], [(116) and (112)] and [(018) and (214)] of pure $BiFeO_3$ shifted gradually to higher 2θ values till 7% Pr-doping and merged in a single broad diffraction peak in 10% Pr-doped $BiFeO_3$ nanoparticles. This observed peak shifting and merging in the XRD pattern of $Bi_{1-X}Pr_XFeO_3$ nanoparticles with increasing Pr concentration suggests that there are partial structural changes occurs in the $BiFeO_3$ matrix. It reveals that Pr^{3+} ions occupy the Bi site in $BiFeO_3$ since the Shannon Prewitt ionic radius of Pr^{3+} (1.12 Å, coordination no. 8) and for Bi^{3+} (1.17 Å, coordination no. 8) are comparable within Goldschmidt tolerance limit [27]. This result suggests strain in lattice parameter and the rhombohedral structure is distorted by Pr-substitution. There exists a structural transformation and a gradual change in lattice constant from rhombohedral structure (*R*3*c*) to triclinic structure (*P*1), which is consistent with Sm-doped $BiFeO_3$ [28,29].

Further, a similar effect of doping of rare earth ions in $BiFeO_3$ has been reported by various researchers [16,30-35]. In addition, the crystalline sizes calculated from the XRD patterns using Scherrer's formula were found to be 32, 26, 24 and 21 nm for $BiFeO_3$, $Bi_{0.95}Pr_{0.05}FeO_3$, $Bi_{0.93}Pr_{0.07}FeO_3$ and $Bi_{0.90}Pr_{0.10}FeO_3$, respectively. With increasing Pr-doping content, the crystalline size of Pr-doped $BiFeO_3$ gradually decreases, further indicating structural distortion in $BiFeO_3$ induced by Pr-doping.

Conclusion

In this work, $Bi_{1-x}Pr_xFeO_3$ ($x = 0$, 0.05, 0.07 and 0.10) nanoparticles were synthesized by facile sol-gel auto combustion

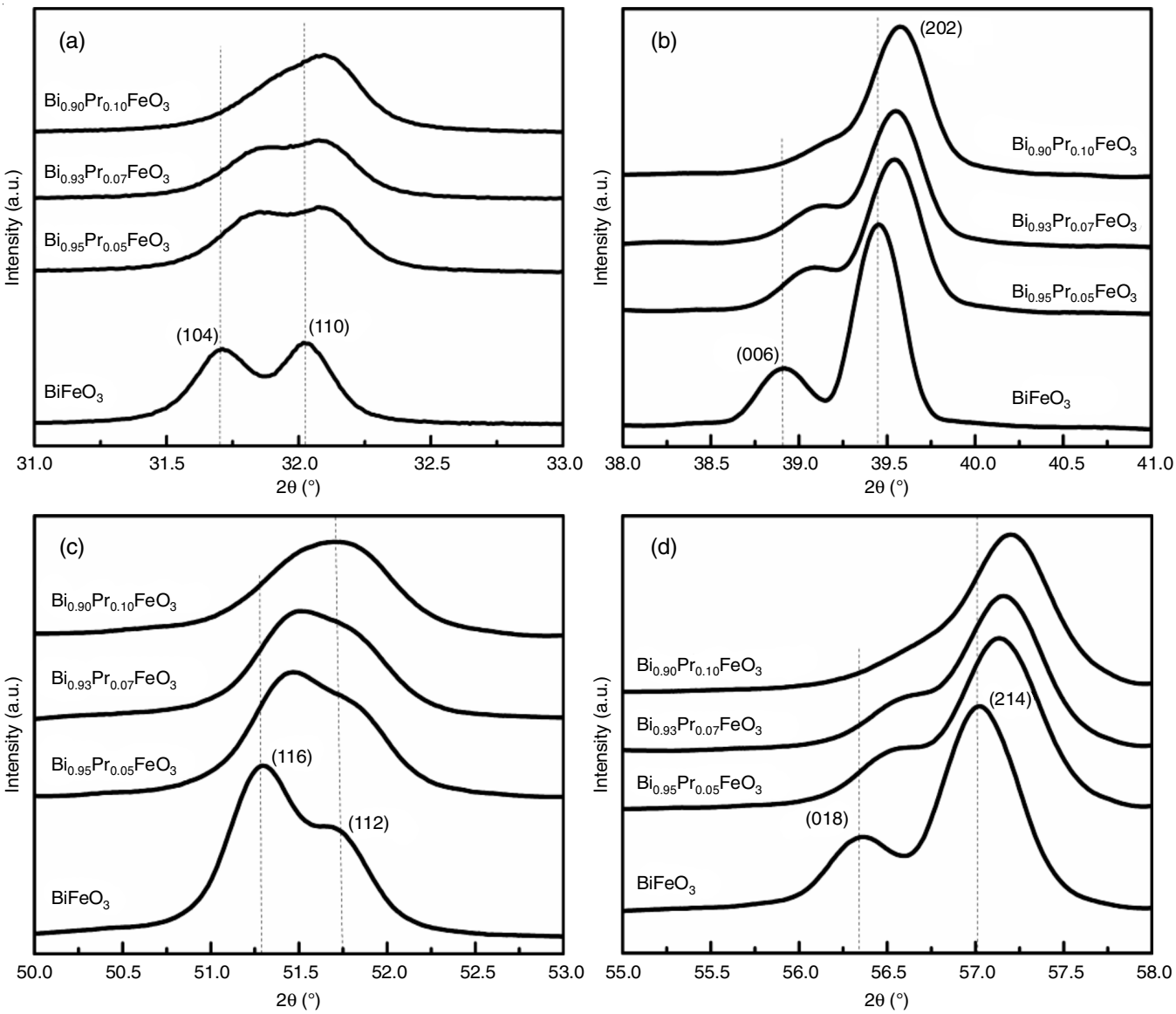

Fig. 5. The magnified XRD patterns in the vicinity of 2θ (a) 32º, (b) 39º, (c) 51º and (d) 57º

route using propylene glycol as a complexing agent after calcination at 400 ºC for 2 h. TGA results showed that the phase formation temperature for $Bi_{1-x}Pr_xFeO_3$ is 400 ºC. TEM results showed that prepared $Bi_{1-x}Pr_xFeO_3$ nanoparticles are nearly spherical in shape with their size ranges between 30-80 nm. The XRD analysis shows that pure perovskite rhombohedral $BiFeO_3$ phase with *R*3*c* group and the structural phase transition exits on doping of Pr^{3+} in $BiFeO_3$, as evident from the gradual shifting and merging of diffraction peaks. The average crystalline size was found to be 32 nm, 26 nm, 24 nm and 21 nm for $BiFeO_3$, $Bi_{0.95}Pr_{0.05}FeO_3$, $Bi_{0.93}Pr_{0.07}FeO_3$ and $Bi_{0.90}Pr_{0.10}FeO_3$, respectively. The synthesized single phase $Bi_{1-x}Pr_xFeO_3$ nanoparticles can be used in various applications.

ACKNOWLEDGEMENTS

The authors gratefully acknowledge the University Department of Chemistry, Lalit Narayan Mithila University, Darbhanga for providing the research facilities. One of the authors, SKS, acknowledges the University Grant Commission (UGC), New Delhi, India, for providing BSR start-up grants to carry out this research work.

CONFLICT OF INTEREST

The authors declare that there is no conflict of interests regarding the publication of this article.

REFERENCES

1. M. Winkler, K. Geirhos, T. Tyborowski, B. Tóth, D.G. Farkas, J.S. White, T. Ito, S. Krohns, P. Lunkenheimer, S. Bordács and I. Kézsmárki, *Appl. Phys. Lett.*, **125**, 252902 (2024); https://doi.org/10.1063/5.0237659
2. Y. Liu, Y. Wang, J. Ma, S. Li, H. Pan, C.-W. Nan and Y.-H. Lin, *Prog. Mater. Sci.*, **127**, 100943 (2022); https://doi.org/10.1016/j.pmatsci.2022.100943
3. T. Choi, S. Lee, Y.J. Choi, V. Kiryukhin and S.W. Cheong, *Science*, **324**, 63 (2009); https://doi.org/10.1126/science.1168636

4. F. Gao, X.Y. Chen, K.B. Yin, S. Dong, Z.F. Ren, F. Yuan, T. Yu, Z.G. Zou and J.-M. Liu, *Adv. Mater.*, **19**, 2889 (2007); https://doi.org/10.1002/adma.200602377
5. J. Wu, Z. Fan, D. Xiao, J. Zhu and J. Wang, *Prog. Mater. Sci.*, **84**, 335 (2016); https://doi.org/10.1016/j.pmatsci.2016.09.001
6. F. Mushtaq, X. Chen, M. Hoop, H. Torlakcik, E. Pellicer, C. Gattinoni, J. Sort, B.J. Nelson and S. Pané, *iScience*, **4**, 236 (2018); https://doi.org/10.1016/j.isci.2018.06.003
7. S.-M. Lam, J.-C. Sin and A.R. Mohamed, *Mater. Res. Bull.*, **90**, 15 (2017); https://doi.org/10.1016/j.materresbull.2016.12.052
8. A. Haruna, I. Abdulkadir and S.O. Idris, *Heliyon*, **6**, e03237 (2020); https://doi.org/10.1016/j.heliyon.2020.e03237
9. S. Bharathkumar, M. Sakar, J. Archana, M. Navaneethan and S. Balakumar, *Chemosphere*, **284**, 131280 (2021); https://doi.org/10.1016/j.chemosphere.2021.131280
10. I. Papadas, J.A. Christodoulides, G. Kioseoglou and G.S. Armatas, *J. Mater. Chem. A Mater. Energy Sustain.*, **3**, 1587 (2015); https://doi.org/10.1039/C4TA05272B
11. J.K. Reddy, B. Srinivas, V.D. Kumari and M. Subrahmanyam, *ChemCatChem*, **1**, 492 (2009); https://doi.org/10.1002/cctc.200900189
12. S.X. Wu, J. Fang, X. Xu, Z. Liu, X. Zhu and W. Xu, *Photochem. Photobiol.*, **88**, 1205 (2012); https://doi.org/10.1111/j.1751-1097.2012.01164.x
13. Z.M. El-Bahy, A.A. Ismail and R.M. Mohamed, *J. Hazard. Mater.*, **166**, 138 (2009); https://doi.org/10.1016/j.jhazmat.2008.11.022
14. M. Sakar, S. Balakumar, P. Saravanan and S. Bharathkumar, *Nanoscale*, **7**, 10667 (2015); https://doi.org/10.1039/C5NR01079A
15. Y.L. Pei and C.L. Zhang, *J. Alloys Compd.*, **570**, 57 (2013); https://doi.org/10.1016/j.jallcom.2013.03.176
16. N. Zhang, D. Chen, F. Niu, S. Wang, L. Qin and Y. Huang, *Sci. Rep.*, **6**, 26467 (2016); https://doi.org/10.1038/srep26467
17. S.J.J. Kay, N. Chidhambaram, A. Thirumurugan, S. Shanavas, P. Sakthivel and R.S.R. Isaac, *J. Mater. Sci.: Mater. Electron*., **34**, 2034 (2023); https://doi.org/10.1007/s10854-023-11486-4
18. S. Kharbanda, N. Dhanda, A.-C.A. Sun, A. Thakur and P. Thakur, *J. Magn. Magn. Mater.*, **572**, 170569 (2023); https://doi.org/10.1016/j.jmmm.2023.170569
19. Q. Zhang, D. Sando and V. Nagarajan, *J. Mater. Chem. C Mater. Opt. Electron. Devices*, **4**, 4092 (2016); https://doi.org/10.1039/C6TC00243A
20. M. Verma, A. Kumar, V.K. Thakur, A. Maurya, S. Kumar, S. Singh and S.K. Srivastva, *Journal of Sol-Gel Technology*, **113**, 356 (2024); https://doi.org/10.1007/s10971-024-06607-2
21. T.J. Park, G. Papaefthymiou, A.J. Viescas, A.R. Moodenbaugh and S.S. Wong, *Nano Lett.*, **7**, 766 (2007); https://doi.org/10.1021/nl063039w
22. T. Liu, Y. Xu and J. Zhao, *J. Am. Ceram. Soc.*, **93**, 3637 (2010); https://doi.org/10.1111/j.1551-2916.2010.03945.x
23. T. Liu, Y. Xu, S. Feng and J. Zhao, *J. Am. Ceram. Soc.*, **94**, 3060 (2011); https://doi.org/10.1111/j.1551-2916.2011.04536.x
24. S. Ghosh, S. Dasgupta, A. Sen and H.S. Maiti, *J. Am. Ceram. Soc.*, **88**, 1349 (2005); https://doi.org/10.1111/j.1551-2916.2005.00306.x
25. S.K. Srivastav and N.S. Gajbhiye, *J. Am. Ceram. Soc.*, **95**, 3678 (2012); https://doi.org/10.1111/j.1551-2916.2012.05411.x
26. G.V. Rao, C.N.R. Rao and J.R. Ferraro, *Appl. Spectrosc.*, **24**, 436 (1970); https://doi.org/10.1366/000370270774371426
27. R.D. Shannon and C.T. Prewitt, *Acta Crystallogr. B*, **25**, 925 (1969); https://doi.org/10.1107/S0567740869003220
28. G.L. Yuan and S.W. Or, *J. Appl. Phys.*, **100**, 024109 (2006); https://doi.org/10.1063/1.2220642
29. G.L. Yuan, S.W. Or and H.L.W. Chan, *J. Appl. Phys.*, **101**, 064101 (2007); https://doi.org/10.1063/1.2433709
30. V.A. Khomchenko, D.V. Karpinsky, A.L. Kholkin, N.A. Sobolev, G.N. Kakazei, J.P. Araujo, I.O. Troyanchuk, B.F.O. Costa and J.A. Paixão, *J. Appl. Phys.*, **108**, 74109 (2010); https://doi.org/10.1063/1.3486500
31. S. Mohan, B. Subramanian, I. Bhaumik, P.K. Gupta and S.N. Jaisankar, *RSC Adv.*, **4**, 16871 (2014); https://doi.org/10.1039/C4RA00137K
32. R.Q. Guo, L. Fang, W. Dong, F.G. Zheng and M.R. Shen, *J. Phys. Chem. C*, **114**, 21390 (2010); https://doi.org/10.1021/jp104660a
33. J.H. Shah, Z. Huaqian, R. Mehmood, A.I. Channa, J. Kazmi, L. Zhang, F. Rosei and Z. Wang, *J. Mater. Chem. A Mater. Energy Sustain.*, **12**, 11644 (2024); https://doi.org/10.1039/D4TA00886C
34. B. Wang, S.M. Wang, L.X. Gong and Z.F. Zhou, *Ceram. Int.*, **38**, 6643 (2012); https://doi.org/10.1016/j.ceramint.2012.05.051
35. J. Liu, L. Fang, F.G. Zheng, S. Ju and M.G. Shen, *Appl. Phys. Lett.*, **95**, 022511 (2009); https://doi.org/10.1063/1.3183580